

On the Possibility of Melting Water Ice during the Recent Past of Mars: Implications for the Formation of Gullies

L.Lange¹, F.Forget¹

¹Laboratoire de Météorologie Dynamique, Institut Pierre-Simon Laplace (LMD/IPSL), Sorbonne Université, Centre National de la Recherche Scientifique (CNRS), École Polytechnique, École Normale Supérieure (ENS), Paris, France

Key Points:

- Melting of opaque water snow or ice at the surface of Mars over the last 4 million years is prevented by sublimation cooling.
- Melting of subsurface ice in equilibrium with the atmosphere is also unlikely because it is too deep to be warmed enough.
- Subsurface ice brought near the surface by regolith removal is unlikely to melt, as it happens only under unrealistic conditions.

Abstract

The formation of gullies on Mars has often been attributed to the melting of (sub)surface water ice. However, melting-based hypotheses generally overlook key processes: (1) sublimation cooling by latent heat absorption, (2) the non-stability of ice where melting conditions can be reached, and (3) the particular microclimates of gullied slopes. Using state-of-the-art climate simulations, we reassess ice melting scenarios over the past four million years (obliquity $\leq 35^\circ$), beyond the estimated period of gully formation. We find that the melting of opaque water snow or ice at the surface of Mars is unlikely anywhere due to sublimation cooling, while (quasi-) stable subsurface ice is typically too deep to reach melting temperatures. We propose an alternative mechanism in which seasonal CO₂ frost sublimation destabilizes the regolith and brings the underlying water ice close to the surface, allowing rapid heating. Even under these optimal conditions, melting requires unrealistic assumptions. Ice containing a small amount of dust could melt via a solid-state greenhouse effect, but both its possibility and frequency in Mars' recent past remain uncertain.

Plain Language Summary

Mid-latitude slopes on Mars display young surface features known as gullies, which resemble small terrestrial alluvial fans. Owing to this similarity, they were considered evidence for recent liquid water activity, within the last few million years. Several formation models invoke the melting of surface or subsurface water ice. However, these models often neglect three key processes: (1) sublimation consumes latent heat, significantly cooling the ice; (2) water ice is unstable under conditions where melting could occur, since it sublimates first; and (3) gullies typically occur on pole-facing slopes, which are generally too cold to reach melting temperatures. Using new numerical models that account for these effects, we reinvestigate whether ice could have melted recently on Mars. Our results show that fresh snow or opaque ice at the surface cannot melt due to sublimation cooling, and subsurface ice lies too deep to be sufficiently warmed. The most favorable scenario involves ice approaching the surface as seasonal CO₂ frost sublimation erodes the overlying soil. Although this could cause transient heating, melting only occurs under unrealistic assumptions. Slightly dusty ice exposed at the surface could melt at depth, yet the frequency and conditions of its occurrence in Mars' recent past are unknown.

1 Introduction

The detection of liquid water on a planet is of major importance, as its presence on Earth is systematically associated with the existence of life (Rothschild & Mancinelli, 2001). Evidence for past liquid water on Mars comes from dendritic valley networks (e.g., Carr & Clow, 1981), widespread hydrated minerals (Poulet et al., 2005; Carter et al., 2023), and delta-lake systems and fluvial sedimentary conglomerates (Malin & Edgett, 2003; Williams et al., 2013; Mangold et al., 2021). Yet, most of these records date from the Noachian to early Amazonian eras (> 3 billion years), leaving debate about recent liquid water (Fassett & Head, 2008). Although present-day martian surface pressure and temperature can locally exceed the triple point of water (611 Pa, 273.15 K) (Haberle et al., 2001), the atmospheric water vapor content remains extremely low (~ 10 pr- μ m, corresponding to a vapor partial pressure of ~ 0.1 Pa, well below saturation, Smith, 2002). As a consequence of this very low relative humidity (typically of order 0.01%), surface liquid water would undergo rapid evaporation or boiling under typical conditions and cannot be persistently sustained in the absence of continuous replenishment, in contrast to terrestrial environments where evaporative losses are compensated by an active hydrological cycle.

Yet geological observations (see review in Conway & Stillman, 2021) may suggest the presence of liquid water on the surface of Mars in a recent past. Notably, gullies, young

(younger than 4 million years de Haas et al., 2019) surface features found on slopes at mid and high latitudes (Malin & Edgett, 2000) composed of an alcove, a channel, and a depositional apron, are similar to small terrestrial alluvial fans. This analogy initially suggested that these surface features were formed by liquid water (Malin & Edgett, 2000). Since then, many models have suggested that water ice melting at the surface (Malin & Edgett, 2000; Hecht, 2002; Christensen, 2003; Kossacki & Markiewicz, 2004; Williams et al., 2008; Dickson et al., 2023) or subsurface (Costard et al., 2002; Kreslavsky & Head, 2003; Morgan et al., 2010) could trigger the formation/activity of gullies. As observations showed that activity occurs from some gullies during winter (Malin et al., 2006; Dundas et al., 2022), formation processes based on the sublimation of CO₂ ice have been shown to operate today rather than those based on water (see Pilarget & Forget, 2016; Dundas et al., 2019). However, the question remains whether these CO₂-based mechanisms are responsible for the formation of all gullies, given the low number of active gullies today. Recently, Dickson et al. (2023) proposed that Martian gullies may have formed through the melting of water ice within the last million years, with present-day activity driven by the sublimation of CO₂ ice. Using climate simulations at 30° and 35° obliquity (values corresponding to the highest obliquities reached during the last four million years Laskar et al., 2004), they showed that gullies occur in regions where surface soil temperatures exceed 273 K and where the total atmospheric pressures surpass 612 Pa, owing to enhanced surface pressure from the sublimation of CO₂ ice deposits buried at the South Pole during high-obliquity periods (Phillips et al., 2011). Based on these thermal and pressure conditions, they concluded that gullies are associated with environments where melting could potentially occur. However, this scenario faces two main limitations:

1. The calculations by Dickson et al. (2023) did not account for the cooling effect associated with sublimation. As shown by Ingersoll (1970), even if there is no wind to transport water vapor away, the inevitable density contrast between water vapor and the main atmospheric constituent CO₂ is so strong that water vapor cannot accumulate above subliming ice, maintaining a sublimation rate that induces a significant latent heat cooling which prevents the ice temperature from reaching 273.15 K. This conclusion has been confirmed by Schorghofer (2020) and Khuller and Clow (2024). This last study included the effects of the vapor/CO₂ density contrast, gustiness/large-scale wind, and the surface layer's specificity in their water ice sublimation modeling.
2. A source of water, such as subsurface or surface ice, must be available for melting to occur. While Dickson et al. (2023) emphasize that water frost and ground ice are generally observed in terrains where gullies form, we show in this paper that, under recent Martian conditions, water ice is almost inevitably lost wherever temperatures approach 273 K.

Hence, the question of whether melting could have occurred on Mars in the recent past, and whether it could have contributed to the formation of gullies, remains open. This paper aims to investigate, using state-of-the-art Martian climate models, whether the melting of water ice at the surface/subsurface could occur at gully locations in the last 4 million years when the obliquity was $\leq 35^\circ$. The models used are presented in section 2. The possibility of melting ice on the surface and in the subsurface is discussed respectively in section 3.1 and 3.2. We discuss the possibility of melting subsurface ice after erosion of the near-surface in section 3.3. Discussions are led in section 4 and conclusions are drawn in section 5.

2 Methods

2.1 Surface-Atmosphere model

This study uses the 1D and 3D versions of the Mars Planetary Climate Model (PCM, Forget et al., 1999), along with the sub-grid scale slope microclimate parameterization outlined in Lange, Forget, Dupont, et al. (2023). For the 3D simulations, surface properties (albedo, emissivity, thermal inertia) are set to the observations from the Thermal Emission Spectrometer (TES, Putzig & Mellon, 2007). A constant dust opacity of $\tau = 0.2$ is used (a relatively low value that favors higher daytime surface temperature). Paleo-climate simulations at high obliquity include the effect of radiative active clouds (Madeleine et al., 2014). For such simulations, we set the surface pressure to double its present-day value, assuming that CO₂ ice buried beneath the South Pole had entirely sublimed (Phillips et al., 2011). This favors the formation and stability of liquid water. We test three configurations: present-day orbital configuration, 35° obliquity with solar longitude of the perihelion $L_{\text{sp}} = 90^\circ$, and 35° obliquity with $L_{\text{sp}} = 270^\circ$. The eccentricity is set to its present value, as all $\sim 35^\circ$ high-obliquity periods in the last 4 million years occurred with lower eccentricity.

To test the sensitivity of our results, we also used a 1D version of this model derived from the 3D version. The 1D model computes the same physical processes as in the 3D model, but the large-scale dynamics is not modeled. In this model, the surface properties are "free parameters". In our baseline study, we use an albedo of 0.13, a near-surface thermal inertia of 350 J m⁻² K⁻¹ s^{-1/2}, and an emissivity of 1, consistent with observations at gully locations (Harrison et al., 2015). In addition, sensitivity tests were performed by varying the thermal inertia between 50 and 350 J m⁻² K⁻¹ s^{-1/2} and the surface albedo up to 0.3, a range representative of martian bare-surface properties (Putzig & Mellon, 2007). As discussed in section 3.3, lower thermal inertia reduces the amount of energy conducted from the surface to subsurface ice, thereby decreasing subsurface heating and the likelihood of melting. A similar effect is obtained for albedo, as higher values reduce the amount of solar energy absorbed at the surface (not shown). A large-scale wind of 10 m s⁻¹ is prescribed above the boundary layer (a typical value used in 1D studies, e.g., Savijärvi et al., 2024), and the wind profile is calculated by the model (Colaïtis et al., 2013).

As explained in the following sections, the sublimation of water ice, and hence latent heat cooling, is highly sensitive to the near-surface water vapor content. The latter depends strongly on large-scale meteorology and transport processes (Montmessin et al., 2017), which are resolved in the 3D model but not in the 1D model. We therefore represent the lateral transport of atmospheric water in the 1D model by applying a nudging toward a prescribed mean value, while the vertical transport is handled by the boundary-layer and diffusion schemes described in Forget et al. (1999) and Colaïtis et al. (2013). The mixing ratio of water vapor q_{vap} (kg kg⁻¹) given as input to the model at time $t + \Delta t$ (s) is:

$$q_{\text{vap}}(t + \Delta t) = \underbrace{\frac{m_{\text{H}_2\text{O}}g}{P_{\text{surf}}}}_{\text{average mass mixing ratio in the column}} + \left(q_{\text{vap, model}}(t + \Delta t) - \frac{m_{\text{H}_2\text{O}}g}{P_{\text{surf}}} \right) e^{-\frac{\Delta t}{\tau}} \quad (1)$$

where $m_{\text{H}_2\text{O}}$ (kg m⁻²) is the nudging value of the H₂O mass in the column per unit area, $g = 3.72$ m s⁻² the gravity, P_{surf} (Pa) the surface pressure, $q_{\text{vap, model}}(t + \Delta t)$ is the value of the water vapor mixing ratio predicted by the 1D model at time $t + \Delta t$ (Δt being the timestep of the model), and τ (s) is the relaxation time. We also assume that clouds are advected away from the atmospheric column after each time step, so the mixing ratio of water ice in the air is always set to zero before entering a new time step. To deter-

mine the nudging parameters ($m_{\text{H}_2\text{O}}$, τ), we compared the water vapor in the first atmospheric layer of the model (4 m) and the amount of water frost on the surface between the 1D model, for several nudging values, and the 3D model (with similar surface conditions - pressure, surface optical/thermophysical properties). An example is given in Figure 1 for latitude 56.25°N where two values of $m_{\text{H}_2\text{O}}$ were tested: 15 pr- μm , the yearly average value measured by the Thermal Emission Spectrometer TES at this latitude (Smith, 2002), and 25 pr- μm , the maximum value measured by TES over the year at this latitude. Comparison with the 3D model shows that it is necessary to use the maximum value over the year measured by TES at a given latitude to represent the annual water cycle better. By testing several values of the relaxation time τ , we find that $\tau = 1/2$ sol and $\tau = 1/4$ sol (not shown in Figure 1) allow for a realistic representation of the seasonal cycle of water vapor in the atmosphere and frost at the surface, in terms of amplitude and temporal evolution. A value of $\tau = 1/2$ sol is therefore adopted in the simulations presented here.

By testing several values of the relaxation time τ , it appears that choosing a relaxation time of 1/2 sol or 1/4 sol (not shown in Figure 1) is optimal.

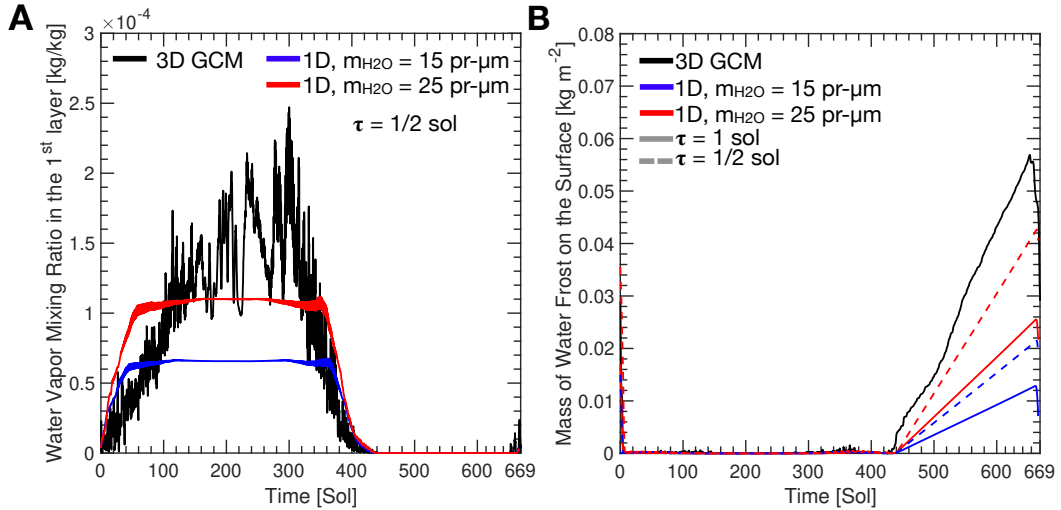


Figure 1. a) Mass mixing ratio of the water vapor in the first layer (~ 4 m) of the model (black curves) at a latitude of 56.25°N (longitudinally averaged), for $m_{\text{H}_2\text{O}} = 15$ pr- μm (blue curve) and $m_{\text{H}_2\text{O}} = 25$ pr- μm (red curve). In these simulations, τ is set to half of a Sol duration. b) Frost thickness predicted by the 3D and the 1D, for the same $m_{\text{H}_2\text{O}}$ as a), and for several relaxation times (one sol for the plain curve, half a sol for the dashed lines).

2.2 Surface ice/frost sublimation model

2.2.1 General description:

The sublimation of water frost/ice on the surface F_{ice} ($\text{kg m}^{-2} \text{s}^{-1}$) is given by (Lange et al., 2024):

$$F_{\text{ice}} = C_q U (\rho_{\text{vap,atm}} - \rho_{\text{sv}}(T_{\text{ice}})) \quad (2)$$

where C_q (unitless) is a moisture transfer coefficient, U (m s^{-1}) is the wind velocity obtained by combining the large-scale (synoptic) wind near the surface with a wind gusti-

ness induced by buoyancy (Colaïtis et al., 2013), $\rho_{\text{vap,atm}}$ (kg m^{-3}) the water vapor density in the near-surface layer (altitude of ~ 4 m), $\rho_{\text{sv}}(T_{\text{ice}})$ (kg m^{-3}) the water vapor density at the icy surface derived from the ice temperature T_{ice} (K) (Murphy & Koop, 2005). C_q depends on the stability of the atmosphere (Colaïtis et al., 2013; Khuller & Clow, 2024; Lange et al., 2024) and is given by:

$$C_q = f_q(Ri) \left(\frac{\kappa^2}{\ln \frac{z_1}{z_0} \ln \frac{z_1}{z_{0q}}} \right) \quad (3)$$

where $f_q(Ri)$ (unitless) is a function of the Richardson number Ri (unitless), κ (unitless) is the von Kármán constant set to 0.4; z_0 (m) is the aerodynamic roughness coefficient extracted from Hébrard et al. (2012), z_{0q} (m) the moisture roughness length derived from the Reynolds and Prandtl numbers (see Eq. 6 of Lange et al., 2024). The stability function $f_q(Ri)$, given by England and McNider (1995), amplifies the flux for an unstable atmosphere, while it reduces it for a stable atmosphere. The Richardson number Ri is the ratio of the buoyancy term to the flow shear term, and depicts the stability of the atmosphere:

$$Ri = \frac{gz_1}{\theta_{\text{v,s}}} \frac{(\theta_{\text{v}}(z_1) - \theta_{\text{v,s}})}{U^2} \quad (4)$$

where $\theta_{\text{v,s}}$ (K) is the virtual surface temperature, $\theta_{\text{v}}(z_1)$ (K) is the virtual temperature at altitude z_1 . This quantity (see expression in Eq. 8 of Lange et al., 2024) represents the temperature that dry air with the same density and pressure as moist air would have. $Ri = 0$ for a neutral atmosphere, $Ri < 0$ for an unstable atmosphere, $Ri > 0$ for a stable atmosphere. Hence, using virtual temperature, the stability of the atmosphere, and thus the sublimation of water ice, is determined by 1) the contrast of density between the near-surface air and atmosphere induced by the difference of temperature and 2) the contrast of density between the moist air at the surface where ice is subliming, and the atmosphere mainly composed of CO_2 . While the latter effect is included in the Richardson number and the stability function in our model, we do not include it when computing the gustiness' wind. This is left as future work as it would require significant changes in the Planetary Boundary Layer within the Mars PCM.

2.2.2 Model validation

Our sublimation model is tested against the latent heat-flux measurements on Earth as presented in Khuller and Clow (2024). These measurements were made at several sites: a glacier in the Purcell Mountains in Canada (Fitzpatrick et al., 2017), oceanic surfaces (Fairall et al., 1996, 2003), an ice-covered lake in the Dry Valleys of Antarctica (Clow et al., 1988) and an underground permafrost tunnel in Alaska (Douglas & Mellon, 2019). The same model's input parameters as those used by Khuller and Clow (2024) are used. The wind used in our model, U , is the one provided by measurements and we do not add the gustiness velocity derived in our model (Colaïtis et al., 2013). To quantify the validity of our model, we use the same metrics as Khuller and Clow (2024), i.e., the root mean square error (RMSE), and the dimensionless index of agreement (d_i) (see their section 5 for definition). Results are shown in Figure 2.

Our model performs reasonably well when modeling the ice sublimation at Purcell Mountains (Figure 2a, $d_i = 65\%$ in our model, 69% for Khuller and Clow (2024)). As in Khuller and Clow (2024), the main discrepancy between our model and measurements comes from the presence of strong low-level katabatic winds which violates some assumptions of the Monin-Obukhov similarity theory on which our model relies. However, our model does not perform well on smooth ocean surfaces (Figure 2b, $d_i = 19\%$ vs 62% for Khuller and Clow (2024)). The main reasons are: 1) the expression of z_{0q} we

used might not be accurate for such smooth surfaces (e.g., Andreas, 1987); 2) the absence of gustiness velocity in our model (for this comparison only), while it might play a significant role, especially for low-wind periods ("free-convective periods"). Note that such conditions are unlikely on Mars at gully locations because of the presence of strong slope winds (Smith & Spiga, 2018; Spiga & Smith, 2018).

Our model performs very well at Mars Analog sites on Earth. Figure 2c shows that our modeled sublimation rates of ice with the conditions of the dry valleys in Antarctica are in excellent agreement with the ones observed ($d_i = 92\%$, similarly to Khuller and Clow (2024)). At the permafrost site in Alaska, for wind velocity of 0.05 m s^{-1} to 0.15 m s^{-1} , and surface roughness between 10 and 15 cm, our model predicts a sublimation rate between 1.6 cm per year to 2.95 cm per year vs 2.1 cm per year measured. Note that other models, except the one from Khuller and Clow (2024), predicted a sublimation rate 4 times higher than the one measured (Douglas & Mellon, 2019).

Hence, our model is validated at Mars Analog sites on Earth and glaciers in Canada, but not on the very smooth oceanic surface, especially during free-convective periods. Given that these conditions are unlikely on Mars at gully sites due to the presence of slope winds, we will consider that our model is reliable for this study, although improvements (especially by adding the effect of water buoyancy on the gustiness) will be considered for future studies.

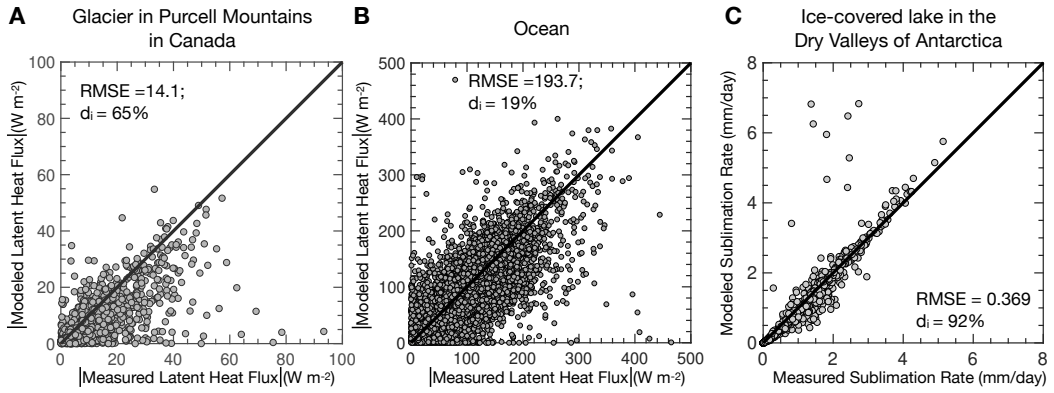


Figure 2. Comparison between modeled vs measured absolute latent heat flux (a, b) and sublimation rate (c) for a) ice glacier in Purcell Mountains (Fitzpatrick et al., 2017), b) oceanic surfaces (Fairall et al., 1996, 2003), and c) an ice-covered lake in the Dry Valleys of Antarctica (Clow et al., 1988). The black line indicates perfect agreement between measured and modeled values. For each case, the root mean square error and dimensionless index of agreement (d_i) (see section 5 of Khuller & Clow, 2024) are given.

2.3 Subsurface ice sublimation model

When ice is buried in the subsurface at depth z_{ice} (m), and when no frost is present at the surface, the water vapor flux from the subsurface water ice to the atmosphere F_{ice} ($\text{kg m}^{-2} \text{ s}^{-1}$) is given by (see demonstration in Appendix A):

$$F_{\text{ice}} = \frac{C_q U}{1 + \frac{C_q U z_{\text{ice}}}{D} \times \frac{1}{1 - \frac{\rho_{\text{vap,atm}}}{\rho_{\text{sv}}(T_{\text{ice}})}}} (\rho_{\text{vap,atm}} - \rho_{\text{sv}}(T_{\text{ice}})) \quad (5)$$

where D ($\text{m}^2 \text{ s}^{-1}$), is the diffusion coefficient through the dry material covering the ice, left as a free parameter here. This expression includes the transport of water vapor from the subsurface ice to the surface, and then the exchange between the surface and the atmosphere with the surface water vapor mixing ratio calculated along the way. The effect of advection within the soil, induced by the gradient of air composition at the subsurface ice interface, is represented by the factor $\frac{1}{1 - \frac{\rho_{\text{vap,atm}}}{\rho_{\text{sv}}}}$ following Hudson et al. (2007). This formulation follows the standard diffusion-limited approach commonly used to describe subsurface ice sublimation in porous media (e.g., Hudson et al., 2007; Schorghofer, 2020). In case frost (either CO_2 or water) is at the surface, the flux is given by:

$$F_{\text{ice}} = \frac{D}{z_{\text{ice}}} \frac{1}{1 - \frac{\rho_{\text{vap,atm}}}{\rho_{\text{sv}}}} (\rho_{\text{sv}}(T_{\text{surf}}) - \rho_{\text{sv}}(T_{\text{ice}})) \quad (6)$$

2.4 Icy (sub)surface thermal model

2.4.1 General description

The evolution of the ice temperature at the surface is governed by the surface energy budget:

$$\rho c_s \frac{\partial T_{\text{ice}}}{\partial t} = (1 - A_{\text{ice}}) F_{\text{rad,sw}}(t) + \epsilon_{\text{ice}} F_{\text{rad,lw}}(t) + F_{\text{ground}}(t) + F_{\text{atm}}(t) + \sum_i L_{\text{H}_2\text{O}} F_{\text{ice}} - \epsilon_{\text{ice}} \sigma T_{\text{ice}}^4(t) \quad (7)$$

where the left member of the equation is the energy of the ice surface layer, with:

- ρ the density of the ice (kg m^{-3});
- c_s the "surface layer" heat capacity per unit area ($\text{J m kg}^{-1} \text{ K}^{-1}$) (heat capacity multiplied by thickness of the first soil layer);
- T_{ice} the ice temperature (K);
- A_{ice} (unitless) the albedo of the ice;
- $F_{\text{rad,sw}}$ the radiative flux at visible wavelengths (W m^{-2});
- ϵ_{ice} (unitless) the surface emissivity (assumed to be equal to the absorptivity);
- $F_{\text{rad,lw}}$ the radiative flux at infrared wavelengths (W m^{-2});
- F_{ground} the soil heat flux due to heat conduction process (W m^{-2});
- F_{atm} the sensible heat flux (W m^{-2});
- $L_{\text{H}_2\text{O}} F_{\text{ice}}$ the sublimation cooling, with $L_{\text{H}_2\text{O}} = 2830 \text{ J kg}^{-1}$ is the latent heat of sublimation of water;
- $\epsilon_{\text{ice}} \sigma T_{\text{ice}}^4$ the radiative cooling of the surface with $\sigma = 5.67 \times 10^{-8} \text{ W m}^{-2} \text{ K}^{-4}$ the Stefan-Boltzmann constant.

A detailed description of all the terms can be found in (Lange, Forget, Dupont, et al., 2023). By default, the emissivity of ice is set to 1, and a broadband albedo of water ice of 0.33 is used. Although this value is quite low for pure H_2O frost, unless it is either mixed with dust (Khuller et al., 2021, for dust concentrations below 1%) or optically thin (Singh & Flanner, 2016, less than a few millimeters thick), it allows us to accurately reproduce the present-day Martian seasonal water cycle (Navarro et al., 2014) and the seasonal evolution of water frost on slopes (Lange, Forget, Dupont, et al., 2023), and remains consistent with observed water frost albedo values, which typically range between 0.2 and 0.6 (Langevin et al., 2005). Varying the albedo used in the simulations do not change the conclusion drawn in this manuscript.

When ice is present in the subsurface, the computation of its temperature is based on a 1D implicit soil model and solves the heat soil conduction:

$$\rho C_p \frac{\partial T_{\text{soil}}}{\partial t} = \frac{\partial}{\partial z} \left(\lambda(z) \frac{\partial T_{\text{soil}}}{\partial z} + L_{\text{H}_2\text{O}} \times F_{\text{ice}} \right) \quad (8)$$

where ρ (kg m^{-3}) is the material's density, and C_p ($\text{J kg}^{-1} \text{K}^{-1}$) is its specific heat, T_{soil} (K) is the subsurface temperature, z (m) is the depth, λ ($\text{W m}^{-1} \text{K}^{-1}$) is the thermal conductivity. The soil grid ranges from 0.2 mm to ~ 20 m, with an irregular grid with a fine resolution ($\leq \text{mm}$) close to the surface. When subsurface ice is present at a depth z_{ice} (m), the thermal inertia (and thereby conductivity) of the corresponding layer and the layers underneath are set to a value I_{ice} ($\text{J m}^{-2} \text{K}^{-1} \text{s}^{-1/2}$). When ice is condensing/subliming, a latent heat flux $L_{\text{H}_2\text{O}} \times F_{\text{ice}}$ is added to the energy budget. By default, we set $I_{\text{ice}} = 1600 \text{ J m}^{-2} \text{K}^{-1} \text{s}^{-1/2}$, a mid-value between completely pore-filled ice (thermal inertia of $\sim 1200 \text{ W m}^{-2} \text{K}^{-1}$; Eq. (26) of Siegler et al., 2012) and massive pure ice (thermal inertia of $\sim 2050 \text{ W m}^{-2} \text{K}^{-1}$ at 180 K; Hobbs, 1974). This value allows for a realistic representation of the present-day Martian CO_2 cycle, which is known to be sensitive to this effect, as well as the distribution of frost on pole-facing slopes (Lange, Forget, Vincendon, et al., 2023).

2.4.2 Model limitations

Although the climate simulations using the model presented above agree with the observed seasonal and spatial distribution of water frost on Mars (Vincendon et al., 2010b; Navarro et al., 2014; Lange, Forget, Dupont, et al., 2023), their surface temperatures (Lange et al., 2024), and the presence of subsurface water ice at high latitudes (Lange, Forget, Vincendon, et al., 2023), the model neglects the penetration of solar radiation into the ice. As shown in the previous section, solar radiation is assumed to be absorbed only at the surface, that is, within the first millimeters of the ice, and not transmitted to deeper layers.

This assumption is consistent with freshly deposited snow mixed with surface dust, which renders it opaque, or with ice covered by a surface dust lag. Near-infrared observations indicate that high-latitude water frost on Mars has typical grain sizes of $10\text{--}100 \mu\text{m}$ (Langevin et al., 2005; Langevin et al., 2007) supporting the use of this assumption for seasonal deposits. The latter situation is expected to occur primarily during the sublimation of dusty ice, since dust sintering tends to clean the remaining ice. Our calculations are thus valid only under this assumption, consistent with the simulations presented in section 3.1, which explore the melting of frost or snow deposited during winter. Other simulations consider ice covered by a few millimeters of dust, which should effectively block solar radiation.

As snow undergoes metamorphism, the grain size is expected to increase, allowing solar flux to penetrate deeper and potentially warming the ice enough to trigger localized melting (see section 4.2). However, the metamorphism rate remains poorly constrained, with estimates ranging from 10–100 years (Clow, 1987) to more than one million years (Bramson et al., 2017), making it difficult to assess whether this process can operate on seasonal timescales. If, nevertheless, coarse-grained snow or relatively clean ice are exposed at the surface, this effect could become significant and potentially allow melting (see discussion in section 4.2).

3 Results

3.1 Melting frost on the surface

We first test the possibility of melting opaque snow/frost on the surface. As theoretically shown by Ingersoll (1970), Schorghofer (2020) and Khuller and Clow (2024), melting of frost/ice on present-day Mars is unlikely because of the cooling of the ice by the latent heat released during the sublimation. Lange et al. (2024) showed that frost temperatures measured on Mars and predicted by the PCM never reach the melting point

of water ice (see their Figure 10). As explained in Lange et al. (2024), the low humidity of the present-day Martian atmosphere limits frost thickness to at most a few millimeters and leads to strong sublimation rates, and thus strong sublimation cooling, preventing frost from reaching high temperatures. To maximize the possibility of surface frost or ice melting, both atmospheric humidity and the solar flux incident on sloped surfaces must be maximized. These conditions occur during the last 4 million years when obliquity reaches 35° and perihelion coincides with northern summer ($L_{sp} = 90^\circ$), which maximizes solar insolation on the northern polar water ice cap. We therefore perform climate simulations and compute water frost thickness and temperature under these optimal conditions (Figure 3). For completeness, we also consider the opposite configuration (obliquity 35° , $L_{sp} = 270^\circ$). We present below results for 30° pole-facing slopes, as they favor frost formation during winter due to low insolation and maximize frost and ice temperatures during spring and summer by receiving higher insolation than flatter surfaces (Costard et al., 2002; Lange et al., 2024). At high obliquity, when the atmosphere is most humid over the last 4 million years, these slopes therefore represent the most favorable configuration for surface melting.

For an obliquity of 35° , water frost forms down to $\sim 20^\circ$ latitude on 30° pole-facing slopes in both hemispheres and closer to the Equator locally in low-thermal inertia regions. The frost thicknesses are larger for $L_{sp} = 90^\circ$ than 270° as a consequence of the difference in global atmospheric humidity between the two simulations. Indeed, for the simulation with $L_{sp} = 90^\circ$, the Northern glacier sublimes more, giving an average humidity value of $260 \text{ pr-}\mu\text{m}$, whereas it is only $58 \text{ pr-}\mu\text{m}$ for $L_{sp} = 270^\circ$. Nevertheless, in both cases, the frost thicknesses are much (~ 30 times for $L_{sp} = 90^\circ$) higher than observed on present-day Mars. As water frost is thicker, it remains longer on the surface and can warm up more as it is more exposed to the sun. In addition, the sublimation flux, and thereby sublimation cooling, is reduced because of the higher near-surface atmospheric humidity. However, as shown in Figures 3a, c, water frost can neither reach the melting temperature, again because of the sublimation cooling by latent heat. The maximum frost temperatures are 271.8 K for $L_{sp} = 90^\circ$, and 264.9 K for $L_{sp} = 270^\circ$. Using the 1D model, we test the effect of the ice properties on the maximum frost temperatures. Even using a low broadband albedo (down to 0.2, representing very dusty ice), the frost temperatures can never reach 273.15 K and melt. Note that using a higher albedo decreases the probability of melting, as frost and ice reflect more solar radiation and absorb less energy. Hence, we confirm that the melting of water frost/ ice on the surface is unlikely because of the sublimation cooling, even at high obliquity when the planet is much wetter, refuting the conclusions of Kossacki and Markiewicz (2004) and Dickson et al. (2023) which did not include this effect. The possibility of lowering the melting temperatures in the presence of salts and of melting within the ice at depth due to a solid-state greenhouse effect are discussed in section 4.

3.2 Melting subsurface water ice in equilibrium with the atmosphere

Costard et al. (2002) proposed that subsurface ice present even below the diurnal thermal skin depth could melt as diurnal mean temperatures on 30° pole-facing slopes at mid-latitudes exceed 273.15 K at high obliquity. However, Mellon and Phillips (2001) reported that such ice should disappear completely before reaching the melting temperature. To test this possibility, we first compute the depth at which the subsurface is in equilibrium with the water vapor content in the atmosphere for present-day and 35° obliquity with the 3D model. Subsurface ice is in equilibrium with the water vapor content in the atmosphere at depth z_{ice} (m) when the yearly-averaged water vapor density at the surface is equal to the one at the ice table (Mellon et al., 2004; Schorghofer & Aharonson, 2005). The thermal inertia of the layer below this depth is set to $1600 \text{ J m}^{-2} \text{ K}^{-1} \text{ s}^{-1/2}$. Simulations are relaunched to include the effect of this large thermal inertia on the soil temperatures, and the process is iterated until the equilibrium depth has converged. Equilibrium depths for present-day climate and 35° obliquity are presented in Figure 4.

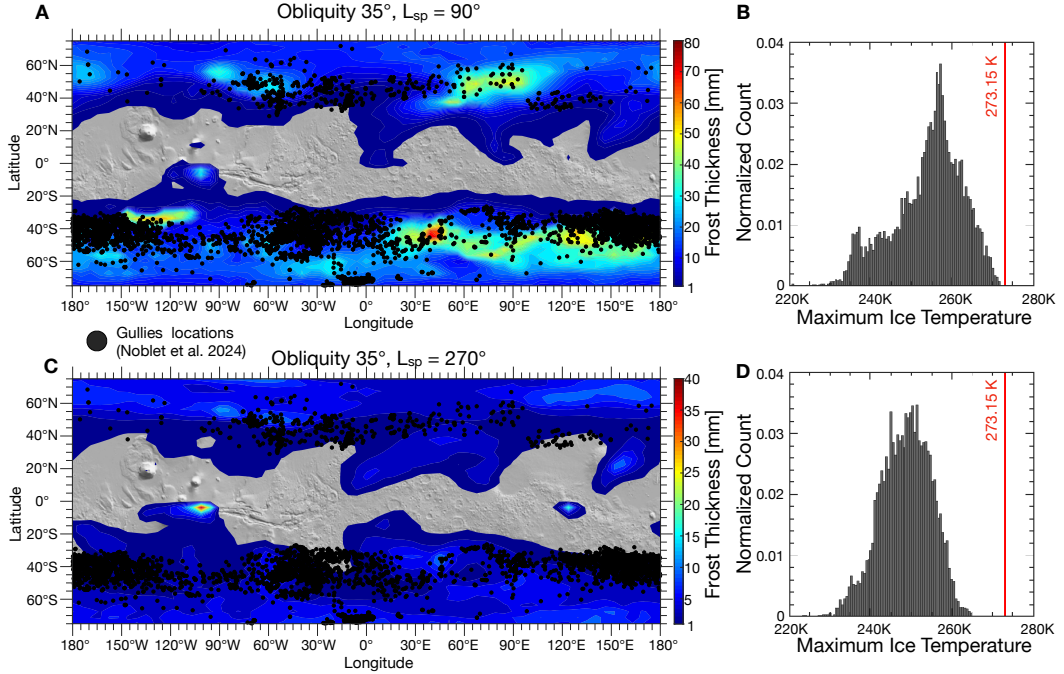


Figure 3. *Left column:* Maximum thickness of seasonal frost on 30° pole-facing slopes for an obliquity of 35° and $L_{sp} = 90^\circ$ (a), and $L_{sp} = 270^\circ$ (c) Gullies locations from Noblet et al. (2024) are reported by black dots. *Right column:* Maximum temperatures of seasonal frost on 30° pole-facing slopes for an obliquity of 35° and $L_{sp} = 90^\circ$ (b), and $L_{sp} = 270^\circ$ (d). The red line is the melting point of water ice (273.15 K).

The distribution of subsurface ice on pole-facing slopes for the present climate is discussed in Lange, Forget, Vincendon, et al. (2023). At an obliquity of 35° and $L_{sp} = 90^\circ$, the modeled atmospheric humidity is so high that ice remains in equilibrium with the water vapor content in the atmosphere within the upper centimeters of the surface (Figure 4c) at tropical latitudes and locally in dusty equatorial regions. These depths do not necessarily imply the presence of massive ice deposits at these latitudes and depths: they rather indicate that if such ice exists, it is in equilibrium with the water vapor content in the atmosphere. However, even if massive ice is not present, ice can still form within the pores of the regolith. At an obliquity of 35° and $L_{sp} = 270^\circ$, ice is not in equilibrium with the water vapor content in the atmosphere near the surface, but is in equilibrium at greater depths (> 70 cm) due to lower atmospheric humidity.

In all cases, we find that subsurface ice does not reach the melting temperature: the maximum temperature is 259 K, which occurs at an obliquity of 35° and $L_{sp} = 90^\circ$, when the ice is closest to the surface (Figures 4c, d). For the present-day, the maximum subsurface ice temperature is 222.4 K and is 240.5 K at obliquity of 35°, $L_{sp} = 270^\circ$. This result is expected: when stable, ice is generally not exposed to large diurnal or seasonal temperature variations; otherwise, sublimation would be too significant, preventing it from remaining in its equilibrium zone. Changing the thermal inertia of subsurface ice from 1600 to 800 $J m^{-2} K^{-1} s^{-1/2}$ for instance does not change our conclusions: if a lower thermal inertia is used, the ice buries itself deeper than it would with a higher thermal inertia. This feedback mechanism ensures that the ice remains cold on average throughout the year. Finally, we have checked whether pore-filling ice or subsurface frost can melt. In all cases, the quantity of frost is too low and it sublimes very quickly before reach-

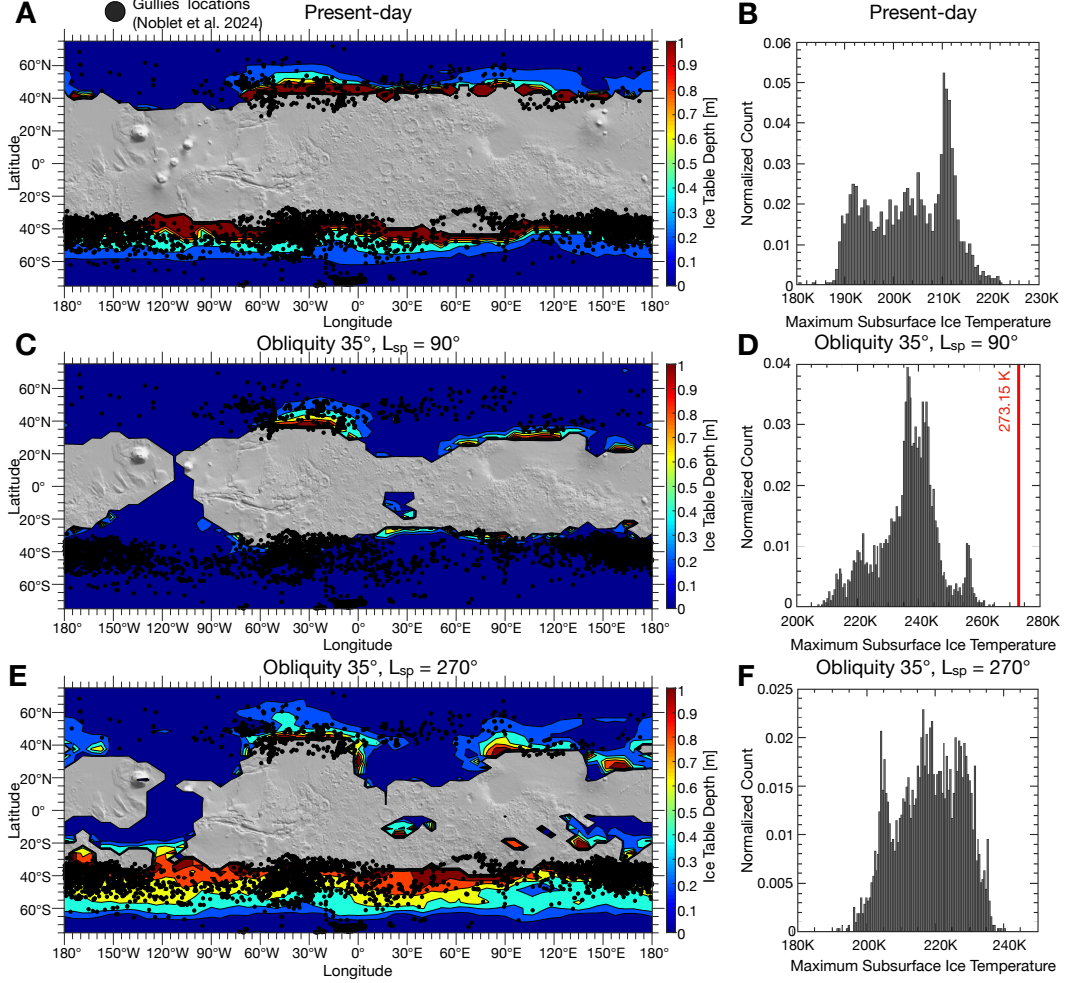


Figure 4. *Left column:* Depth at which ice table beneath a 30° pole-facing slope for present-day (a), an obliquity of 35° and $L_{sp} = 90^\circ$ (c), and $L_{sp} = 270^\circ$ (e). Gullies' location from Noblet et al. (2024) is reported by black dots. *Right column:* Maximum temperatures of the upper surface of the ice table for present-day (b), an obliquity of 35° and $L_{sp} = 90^\circ$ (d), and $L_{sp} = 270^\circ$ (f). The red line is the melting point of water ice (273.15 K).

ing the melting temperature of ice. We conclude that when ice is at its equilibrium depth, it cannot melt.

3.3 Melting suddenly warmed subsurface water ice

As shown previously, ice at the surface can not melt because of the latent heat cooling induced by the significant sublimation rate. Ice buried beneath the regolith can be protected from sublimation and thereby latent heat cooling, but ground ice in equilibrium with the atmosphere is too deep to be warmed enough and melt. Can we imagine a process that would allow stable ice on Mars to be exposed to an unusual or even sudden heating? For instance, a well-known case on Mars is when a meteoritic impact in the mid-latitude excavates regolith and sometime exposes water ice (Byrne et al., 2009), but such events are rare and local. However, another process that can play this role exist on Mars and it is precisely active on gullied slopes: there, at the end of winter, seasonal CO₂ ice sublimation has been shown to sometime destabilizes the surface regolith

material (Dundas et al., 2012; Pilorget & Forget, 2016), inducing a dry debris flow, that is now thought to be at the origin of most gully activities on Mars today. When such a process occur, the local water ice table (almost always present on known gullied slopes) can suddenly be exposed at the surface (Khuller & Christensen, 2021) or left with only a thin layer of dry soil above it (Pilorget & Forget, 2016), experiencing rapid heating when the surface is heated by the sun but without losing too much latent heat thanks to the thin soil cover between the water ice and the atmosphere. We also note that, in this scenario, water frost trapped at the base of the seasonal CO₂ ice layer could in principle experience enhanced springtime heating, as solar radiation can penetrate the translucent CO₂ ice. However, as shown by Pilorget et al. (2011) and Pilorget and Forget (2016), the temperatures reached at the CO₂ ice-soil interface, where such water frost would be located, remain below ~ 160 K, well below the melting point of water, and therefore do not allow liquid water formation.

To test whether subsurface ice can melt under the latter conditions, we use our 1D model to simulate its evolution after surface erosion (inputs in Table 1). Subsurface ice is initially placed at depth z_{ice} , and the layer below are assigned ice thermal properties. The model equilibrates temperatures over 10 years. After that, during the CO₂ sublimation in winter, ice is moved from z_{ice} to $(1-\alpha)z_{\text{ice}}$, with α being an excavation factor between 0 (no excavation) and 1 (ice exposed at the surface). The removed soil thickness αz_{ice} defines the new surface, setting the soil temperature there. The model then calculates sublimation, temperature, and ice depth evolution over 2 years (1-minute timestep). We will only consider here the case in which ice is still opaque as it is covered by a thin layer of dust. Indeed, our model might not be appropriate to study the case of suddenly exposed ice, when solar absorption could have a significant impact on the possibility of melting (see section 4.2). Results of our experience are shown in Figure 5.

Parameter	Value/Range of values
Obliquity	25.2°, 35°
Solar Longitude of Perihelion	270°
Eccentricity	0.0934
Latitude	30°S, 40°S, 50 °S
Slope angle	0°-30°, 10° step, facing North and South
Subsurface ice initial depth z_{ice}	0.2 – 1 m
Albedo of bare ground	0.13
Thermal inertia of dry soil	50 - 350 J m ⁻² K ⁻¹ s ^{-1/2}
Surface pressure (present-day)	400 - 800 Pa
Vapor in the atmosphere (present-day)	10 pr- μ m
Surface pressure (35° obliquity)	800 - 1600 Pa
Vapor in the atmosphere (35° obliquity)	260 pr- μ m
Diffusion coefficient	4×10^{-4} , 1×10^{-5} m ² s ⁻¹
Excavation factor α	0.9, 0.99, 0.999

Table 1. Set-up for the simulations performed in section 3.3. Simulations are done in the South as it is where most of the gullies are observed.

3.3.1 Present-day:

For current orbital conditions, the temperature of the subsurface ice after being destabilized never reaches 273.15 K. The median temperature reached is 248 K, and the maximum temperature is 271.8 K. We find that the maximum temperature achieved depends on surface and subsurface properties:

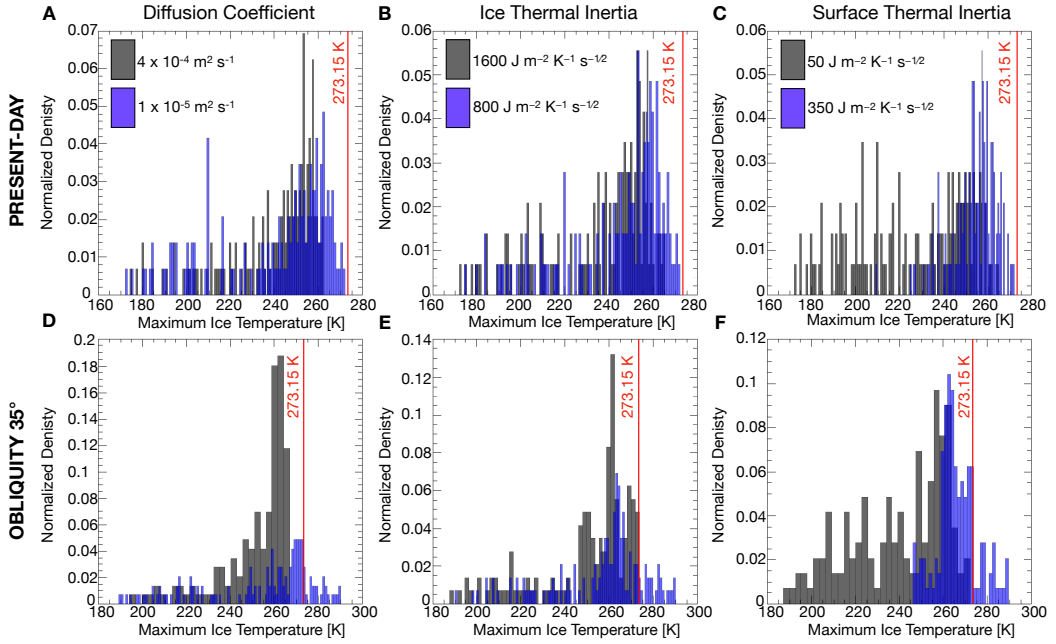


Figure 5. Distribution of maximum subsurface ice temperatures simulated after surface erosion. Each count represents a simulation with parameters detailed in Table 1, normalized by the total number of simulations (288). Top panels (a–c) correspond to present-day obliquity and water vapor content, while bottom panels (d–f) correspond to 35° obliquity. Panels a and c illustrate sensitivity to the dry soil diffusion coefficient; b and e to ice thermal inertia; c and f to dry soil thermal inertia. Only ice temperatures beneath 30° slopes are shown, as this configuration produces the highest ice temperatures during summer. Temperatures may exceed the melting point because the latent heat of melting is not included in our model once ice temperatures exceed 273.15 K.

- Ice must be close to the surface, otherwise it will be too deep to be heated by the diurnal/seasonal thermal heat wave during summer. However, the ice cannot be at too shallow a depth otherwise sublimation cooling would reduce the ice temperature. As shown analytically by Schorghofer (2020) and confirmed numerically by our simulations, ice located a few centimeters below the surface represents an optimum configuration that maximizes heating while minimizing latent heat cooling.
- The ice temperature is higher when the covering dry soil diffusion coefficient is low (Figure 5a). If the diffusion coefficient is too high, then the sublimation of the ice is strong and the sublimation cooling prevents reaching high ice temperatures. According to Hudson et al. (2007), the possible range of diffusion coefficients on present-day Mars is between $10^{-5} \text{ m}^2 \text{ s}^{-1}$ (compacted dust) and $4 \times 10^{-4} \text{ m}^2 \text{ s}^{-1}$ (regolith). In comparison, effective diffusion coefficient of the ice-free permafrost on Earth is about $10^{-6} \text{ m}^2 \text{ s}^{-1}$ (McKay et al., 1998; Douglas & Mellon, 2019). Within the range of typical Martian diffusion coefficients, our model does not predict ice melting (Figure 5a).
- The thermal inertia of the ice must be low. This point will be discussed below, but even when using unrealistically low thermal inertia values (e.g., $< 100 \text{ J m}^{-2} \text{ K}^{-1} \text{ s}^{-1/2}$), our model does not predict the melting of the ice (Figure 5b).
- The thermal inertia of dry soil, and thus its conductivity, must be high. More conductive soil allows heat to penetrate deeper, reaching buried ice. However, higher

conductivity also reduces the diurnal temperature peak, lowering the likelihood of melting. In any case, no melting occurs in our model (Figure 5c). Note that higher conductivity requires cementation between soil constituents (Piqueux & Christensen, 2009a, 2009b), which reduces the material's diffusion coefficient, making this condition consistent with the first.

3.3.2 Recent paleoclimates:

During periods of high obliquity, in a few extreme simulations, the modeled maximum subsurface ice temperature (without including the latent heat of fusion) can be higher than 273.15 K (Figure 5), meaning that ice could melt. The melting occurs in the afternoon during summer, over a few days. We estimate (see method in Text S4) that the amount of water formed does not exceed 0.5 mm, i.e., 5% of the volume of the regolith layer above ice (Figure S4). Such value is below the 10% threshold concentration required for debris flow formation (Malin & Edgett, 2000; Costard et al., 2002). Moreover, an analysis of the combined parameters requested to reach melting suggest that they are not realistic. First, melting only occurs if the subsurface diffusion coefficient is less than $10^{-5} \text{ m}^2 \text{ s}^{-1}$ (the maximum temperature of ice covered by a surface with a diffusion coefficient of $4 \times 10^{-4} \text{ m}^2 \text{ s}^{-1}$ is 267 K). Such a low diffusion coefficient is difficult to imagine on Mars due to the low atmospheric pressure. Even assuming a doubling of pressure during periods of high obliquity, the diffusion coefficient remains larger than $4 - 5 \times 10^{-5} \text{ m}^2 \text{ s}^{-1}$ for regolith or dust with micrometer-sized grains (Hudson et al., 2007; Schorghofer, 2020). Our model does not predict the melting of the ice when using these values (not shown). Hudson and Aharonson (2008) experimentally explored the possibility of reducing the soil diffusion coefficient on Mars. Specifically, they found that only mechanically compacted dust, after being buried deeply in the subsurface, may effectively reduce the diffusion coefficient, potentially reaching values as low as $10^{-5} \text{ m}^2 \text{ s}^{-1}$. Therefore, only ancient ice, initially buried at depth before surface erosion, might be likely to melt.

When using such a low diffusion coefficient, our model shows that only ice with thermal inertia of $\leq 800 \text{ J m}^{-2} \text{ K}^{-1} \text{ s}^{-1/2}$ can melt. By varying the thermal inertia of the ice, we observed that a few simulations show melting at $1000 \text{ J m}^{-2} \text{ K}^{-1} \text{ s}^{-1/2}$, but this remains rare. No simulations predict melting for ice with a higher thermal inertia. Such a low thermal inertia for ice is associated with either:

- Snow undergoing metamorphism to ice (thermal inertia values of $\leq 1000 \text{ J m}^{-2} \text{ K}^{-1} \text{ s}^{-1/2}$ are associated with an ice/snow porosity of 50%, see for instance Figure 3 of Bapst et al., 2019). Although the rate of ice metamorphism is not well constrained (see discussion in Khuller & Christensen, 2021), this scenario seems unrealistic. As previously shown, the ice must initially be deeply buried. Bramson et al. (2017) showed that mid-latitude subsurface ice buried beneath a few meters of regolith has a porosity of $\sim 20\%$, translating into a high thermal inertia of more than $1600 \text{ J m}^{-2} \text{ K}^{-1} \text{ s}^{-1/2}$ (Bapst et al., 2019). It is therefore reasonable to assume that ice buried beneath slopes would undergo a similar degree of metamorphism, and hence exhibit a comparably high thermal inertia.
- Ice filling the pores of the regolith (Siegler et al., 2012). However, this scenario is also unrealistic because the material above the ice would need to be compacted, making it difficult to imagine ice in the pores.

For realistic conditions of dry soil, ice thermal inertia and diffusion coefficient, the maximum temperature obtained is below 273 K. Four simulations are within 1 K of the melting temperature of ice, and the rest are colder. Only the simulations with unrealistic properties (thermal inertia lower than $800 \text{ J m}^{-2} \text{ K}^{-1} \text{ s}^{-1/2}$, diffusion coefficient lower than $10^{-5} \text{ m}^2 \text{ s}^{-1}$) leads to the melting of the ground ice. When changing some

parameters (e.g., the albedo of the surface, depth of the ice after the surface removal, or eccentricity of the planet), a few simulations (less than 5% of the total number of simulations performed) manage to reach the melting temperature of water ice. Hence, we conclude that the melting of subsurface ice after being destabilized is very unlikely in the recent past of Mars.

3.3.3 Melting during the formation of a lag-deposit:

Another possibility to have unstable shallow subsurface ice could be during the formation of a lag deposit associated with the sublimation of a dusty ice deposit. As dusty ice sublimes, dust in the ice accumulates on the surface. This process is thought to create lag deposits above the ice, composed of uncompressed (high diffusion coefficient) micron-sized dust particles (with a low thermal inertia). We tested whether melting is possible in this case by modeling the ice temperature beneath a layer of dust (thickness ranging from 1 mm to 1 m, thermal inertia of $50 \text{ J m}^{-2} \text{ K}^{-1} \text{ s}^{-1/2}$, other properties are set as given in Table 1) for present-day and past obliquity. In all of our simulations, the melting temperature is never reached (maximum temperature is 266 K). Indeed, as dust poorly conducts heat, ice must be exposed close to the surface to be effectively warmed. However, because dust has a high diffusion coefficient (down to $4 \times 10^{-5} \text{ m}^2 \text{ s}^{-1}$, Hudson et al., 2007; Hudson & Aharonson, 2008; Schorghofer, 2020), it does not reduce significantly the sublimation of shallow ice and thereby latent heat cooling. Consequently, ice is very unlikely to melt in this case.

4 Discussion

4.1 Effects of salts on the melting of water ice

The presence of salts, widespread on the Martian surface (e.g., Clark, 1981; Hecht et al., 2009; Glavin et al., 2013), in the water ice mixture can reduce the temperature needed to melt. For most of our simulations, frost at the surface, or ice buried in the surface (at equilibrium or unstable) typically have a temperature 20-30 K lower than the melting temperature of pure water ice. The concentration of salt required to reduce the freezing point to such low temperature is significant, up to 40% by weight (Figure 7 of Mellon & Phillips, 2001; Toner et al., 2015). These values are significantly higher than the amount of salts measured in the martian regolith. For example, the abundance of perchlorates measured at various landing sites is < 1 wt.% (see Table 6 in Glavin et al., 2013). Cemented surfaces, such as duricrusts, can contain up to a few percent of salt (e.g., Cabrol et al., 2006), and one can reasonably assume that this amount should be much less within ice deposits formed by snowfall. At such low abundances, the melting temperature is almost similar to that of pure water ice (Toner et al., 2015). Therefore, while localized melting at the salt–ice interface may occur, the formation of substantial brine volumes, and hence their influence on gully activity, appears to be limited or unlikely. In a few cases, when the temperature of the ice is within 1-2 K the melting temperature of pure ice, salts concentrations might be high enough to depress the melting temperature and allow the formation of larger brines. Yet, as these cases are rare, we conclude that the formation of large volume brines through the melting of salty ice is unlikely in the recent past of Mars. We acknowledge that a fully self-consistent treatment of the effects of salts on ice sublimation and melting would require explicitly accounting for their impact on thermodynamic properties and mass transfer, including melting temperatures, equilibrium vapor pressures, sublimation fluxes, as well as potential deliquescence (e.g., Chevrier et al., 2022) and changes in the effective diffusion coefficient (e.g., Hudson & Aharonson, 2008) of the porous medium. Such complexity is beyond the scope of the present study and is left for future work. We also acknowledge that highly concentrated salt solutions could form on Mars through deliquescence (e.g., Rivera-Valentín et al., 2020) or repeated thin-film wetting (e.g., Möhlmann, 2008). However, the resulting brines are ex-

pected to occur only in very small amounts (Chevrier & Slank, 2024) and are very unlikely to generate large debris flows such as gullies.

4.2 Melting ice through the solid-state greenhouse effect

As mentioned in section 2.4.2, simulations performed in this study assume that water ice/snow is opaque, meaning all incoming solar radiation is absorbed at the surface of the ice and does not penetrate the ice. In reality, ice can be transparent, allowing photons to heat it from within. If the ice contains impurities such as dust, these impurities can absorb downwelling photons, leading to a solid-state greenhouse effect (Clow, 1987; Williams et al., 2009; Khuller et al., 2024) and heating at depth. In addition, the overlying snowpack is close to saturation. As a result, sublimation and evaporation at depth are reduced, thereby limiting latent heat losses and further promoting melting and the persistence of liquid water. Clow (1987); Williams et al. (2008) and Williams et al. (2009) showed that even a small amount of dust (≤ 1000 parts per million by weight) within the ice is enough to absorb sufficient solar radiation to generate a solid-state greenhouse effect strong enough to melt snow or ice at depth. Notably, Williams et al. (2009) demonstrated that melting could occur if ice with a small amount of dust is exposed at the surface in late spring or summer, when solar heating is at its maximum, producing approximately 1 L m^{-2} of liquid water per day.

Water ice on Mars can contain impurities such as dust. While ice in the polar layered deposits is inferred to contain relatively high dust fractions (more than 10% of the ice content, Plaut et al., 2007; Zuber et al., 2007; Lalich et al., 2019), observations of mid-latitude water ice at impact crater sites where subsurface ice has been excavated (Byrne et al., 2009; Dundas et al., 2018, 2021), at scarps (Dundas et al., 2018), and in the alcoves of some gullies (Khuller & Christensen, 2021) suggest that this ice is relatively clean, with dust contents below 1%. The melting of such ice deposits might occur through the mechanism proposed by Clow (1987); Williams et al. (2008) and Williams et al. (2009). However, since these observations are limited to specific sites rather than all active gully locations (Rangarajan et al., 2024), we cannot draw quantitative conclusions about how frequently this process may contribute to gully activity, nor about the prevalence of melting driven by this mechanism in Mars' recent past. Moreover, the potential for melting also depends on ice microphysics, notably the grain size (as larger grains enhance deeper solar absorption) and the dust content within the ice. Given the limited constraints on Martian ice metamorphism and the past dust cycle (Kahre et al., 2017), we are therefore unable to estimate the frequency of melting episodes resulting from the solid-state greenhouse effect in Mars' recent history, which remains the subject of ongoing investigation (e.g., Khuller et al., 2024).

4.3 Other mechanisms

Other mechanisms have been proposed to promote ice melting. The first concerns the radiative effect induced by the geometry of gully alcoves. These alcoves create shading that forms cold traps where volatiles, such as CO_2 and water, preferentially condense during winter. When exposed to sunlight, these points can become warm due to direct insolation, limited radiative cooling to the sky by surrounding walls, and radiative fluxes emitted by these walls. Hecht (2002) suggested that these effects, combined with a clear sky and a poorly conductive surface, could allow ice to melt in these locations. However, the effect strongly depends on geometry, particularly the depth-to-width ratio of the alcove, which controls the balance between maximizing insolation and minimizing radiative losses. Schorghofer et al. (2019), using a more complete model including shadowing and radiative coupling, showed that while these alcoves promote preferential condensation of water frost, the frost disappears before melting occurs. Since these simulations were performed for a single crater (Palikir Crater), new simulations at active gully sites

would be required to quantitatively assess the influence of these geometric effects on gully activity.

A second possibility is melting of subsurface ice due to geothermal heating. Mellon and Phillips (2001) showed that a combination of typical geothermal fluxes and a poorly conducting soil layer of 100 m thickness could allow the formation of subsurface aquifers. Wood and Griffiths (2007) further suggested that pressure variations linked to orbital cycles (Buhler & Piqueux, 2021) could reduce the thermal conductivity of the regolith, leading to deeper warming of subsurface ice through geothermal heat trapping, thus promoting melting as proposed by Mellon and Phillips (2001). However, as noted by Mellon and Phillips (2001), this mechanism relies on the presence of a thick, poorly conducting regolith layer. Although the thickness of the Martian regolith is poorly constrained, observations at the InSight landing site show rocks a few meters below the surface (Golombek et al., 2020), which contradicts the assumption of a thick regolith layer, although this may not be representative of the entire planet. Furthermore, no observations currently support the existence of subsurface aquifers, rendering this mechanism uncertain.

The last mechanism involves the excavation of subsurface ice by impacts (Byrne et al., 2009). The energy delivered by the impactor could be sufficient to melt buried ice locally. Modeling by Reufer et al. (2010), based on the impacts detected by Byrne et al. (2009), indicates that melting only occurs in the largest craters, where the impactor penetrates deeply into the ground ice (at least \sim 1 m). However, no mud, cemented material, or flow-like features generated by this liquid water have been observed (Dundas et al., 2014), and due to the spatial and temporal rarity of such impacts, liquid water formation via this mechanism would remain a rare phenomenon.

5 Conclusions

The objectives of this paper were to discuss the possibility of melting opaque water ice/snow at the surface or in the subsurface of Mars during the last 4 million years when the obliquity of the planet was lower than 35°. The main conclusions of this investigation are:

1. Fresh deposited water frost/snow at the surface cannot melt on present-day Mars and during recent periods of high obliquity (up to 35°) because of the significant sublimation cooling which prevents ice from reaching 273.15 K.
2. Subsurface water ice at its equilibrium depth can not melt as it is too deep to be efficiently warmed.
3. Subsurface ice destabilized after an erosion of the surficial regolith (induced by CO₂ ice sublimation for instance) is unlikely to melt since melting requires unrealistic conditions (porous ice that has only been half metamorphised, while being deeply buried and thus old).
4. Melting during the burial of the ice is also unlikely as the regolith/dust can not act as an efficient diffusion barrier.
5. The presence of salts could allow the formation of brines at the salt–ice interface. However, the volume of the liquid brines would be low given the low concentration of salt that does not significantly depress the melting temperature of ice.
6. Exposure of ice with a small amount of dust could melt because of the solid-state greenhouse effect induced by the absorption of solar radiation by dust (Clow, 1987; Williams et al., 2008; Williams et al., 2009). However, we can not draw quantitative conclusions about the occurrence of such a mechanism in the recent past of Mars given the sparse observations of such ice at gully locations (Khuller & Christensen, 2021; Rangarajan et al., 2024).

Although our study focuses on the recent past of Mars, it cannot be generalized to earlier times, particularly in periods of very high obliquity ($\sim 45^\circ$), when the planet was even more humid, cloudy and likely dustier, possibly allowing ice to melt. Finally, improved constraints on Martian ice metamorphism, including the evolution of grain size, porosity, and dust content over time, are essential to better assess the potential for melting in both recent and earlier climatic periods. Such knowledge would refine our understanding of the conditions under which surface and subsurface ice could transiently produce liquid water on Mars.

Conflict of Interest

The authors declare no conflicts of interest relevant to this study.

Open Research

- Data: Data files for figures used in this analysis are available in a public repository, see Lange and Forget (2025).
- Software: The Mars PCM used in this work can be downloaded with documentation at <https://svn.lmd.jussieu.fr/Planeto/trunk/LMDZ.MARS/>. More information and documentation are available at <http://www-planets.lmd.jussieu.fr>. (Forget et al., 2025)

Acknowledgments

This project has received funding from the European Research Council (ERC) under the European Union’s Horizon 2020 research and innovation program (grant agreement No 835275, project ”Mars Through Time”). Mars PCM simulations were done thanks to the High-Performance Computing (HPC) resources of Centre Informatique National de l’Enseignement Supérieur (CINES) under the allocation n°A0100110391 made by Grand Equipement National de Calcul Intensif (GENCI); to the IPSL Data and Computing Center ESPRI which is supported by CNRS, Sorbonne Université, CNES and Ecole Polytechnique, and to the SACADO MeSU platform at Sorbonne Université. The authors acknowledge A.Khuller, N.Schorghofer, C.Freissinet, V.Chevrier, B.Jakosky for insightful discussions, M.Sorie and the two reviewers for their constructive comments.

Appendix A Expression of the sublimation flux of subsurface water ice:

The determination of the sublimation rate of subsurface ice is made using similar arguments to those presented in Schorghofer (2020). The flux of vapor in the soil between subsurface ice subliming at depth z_{ice} (m) and the surface ($F_{\text{surface} \leftarrow \text{surface}}$, in $\text{kg m}^{-2} \text{ s}^{-1}$) is given by (Hudson et al., 2007):

$$F_{\text{subsurface ice} \leftarrow \text{surface}} = \frac{D}{z_{\text{ice}}} \frac{1}{1 - \frac{\rho_{\text{vap,atm}}}{\rho_{\text{sv}}(T_{\text{ice}})}} (\rho_{\text{sv}}(T_{\text{surf}}) - \rho_{\text{vap,surf}}) \quad (\text{A1})$$

where $\rho_{\text{vap,surf}}$ is the near-surface vapor density (kg m^{-3}), and the rest of the variables are been defined in section 2.3.

The flux of water vapor between the surface and the atmosphere $F_{\text{surface} \leftarrow \text{atmosphere}}$, in $\text{kg m}^{-2} \text{ s}^{-1}$, is given by:

$$F_{\text{surface} \leftarrow \text{atmosphere}} = C_q U (\rho_{\text{vap,atm}} - \rho_{\text{vap,surf}}) \quad (\text{A2})$$

Mass conservation requires that $F_{\text{surface} \leftrightarrow \text{surface}} = F_{\text{surface} \leftrightarrow \text{atmosphere}}$. Let's define:

$$R = \frac{C_q U z_{\text{ice}}}{D} \left(1 - \frac{\rho_{\text{vap,atm}}}{\rho_{\text{sv}}(T_{\text{ice}})} \right) \quad (\text{A3})$$

After some development, one has:

$$\rho_{\text{vap,surf}} = \frac{\rho_{\text{sv}}(T_{\text{ice}}) + R \rho_{\text{vap,atm}}}{1 + R} \quad (\text{A4})$$

Reinjecting this expression in Eq. A1 or A2 leads to the expression given in Eq. 5.

References

Andreas, E. L. (1987). A theory for the scalar roughness and the scalar transfer coefficients over snow and sea ice. *Boundary-Layer Meteorology*, 38(1–2), 159–184. doi: 10.1007/bf00121562

Bapst, J., Byrne, S., Bandfield, J. L., & Hayne, P. O. (2019). Thermophysical Properties of the North Polar Residual Cap using Mars Global Surveyor Thermal Emission Spectrometer. *Journal of Geophysical Research: Planets*, 124(5), 1315–1330. doi: 10.1029/2018JE005786

Bramson, A. M., Byrne, S., & Bapst, J. (2017). Preservation of Midlatitude Ice Sheets on Mars. *Journal of Geophysical Research: Planets*, 122(11), 2250–2266. doi: 10.1002/2017je005357

Buhler, P. B., & Piqueux, S. (2021). Obliquity-driven co2 exchange between mars' atmosphere, regolith, and polar cap. *Journal of Geophysical Research: Planets*, 126(5), e2020JE006759. (e2020JE006759 2020JE006759) doi: 10.1029/2020JE006759

Byrne, S., Dundas, C. M., Kennedy, M. R., Mellon, M. T., McEwen, A. S., Cull, S. C., ... Seelos, F. P. (2009). Distribution of Mid-Latitude Ground Ice on Mars from New Impact Craters. *Science*, 325(5948), 1674–1676. doi: 10.1126/science.1175307

Cabrol, N. A., Farmer, J. D., Grin, E. A., Richter, L., Soderblom, L., Li, R., ... Arvidson, R. E. (2006). Aqueous processes at Gusev crater inferred from physical properties of rocks and soils along the Spirit traverse. *Journal of Geophysical Research: Planets*, 111(E2). doi: 10.1029/2005je002490

Carr, M. H., & Clow, G. D. (1981). Martian channels and valleys: Their characteristics, distribution, and age. *Icarus*, 48(1), 91–117. doi: 10.1016/0019-1035(81)90156-1

Carter, J., Riu, L., Poulet, F., Bibring, J.-P., Langevin, Y., & Gondet, B. (2023). A Mars orbital catalog of aqueous alteration signatures (MOCAAS). *Icarus*, 389, 115164. doi: 10.1016/j.icarus.2022.115164

Chevrier, V. F., Fitting, A., Elsenousy, A., & Rivera-Valentín, E. G. (2022). Thermodynamic modelling of perchlorate/chloride and perchlorate/chlorate deliquescence at Mars-relevant temperatures. *Geochimica et Cosmochimica Acta*, 333, 56–74. doi: 10.1016/j.gca.2022.06.011

Chevrier, V. F., & Slank, R. A. (2024). The elusive nature of Martian liquid brines. *Proceedings of the National Academy of Sciences*, 121(52). doi: 10.1073/pnas.2321067121

Christensen, P. R. (2003). Formation of recent martian gullies through melting of extensive water-rich snow deposits. *Nature*, 422(6927), 45–48. doi: 10.1038/nature01436

Clark, B. (1981). The salts of Mars. *Icarus*, 45(2), 370–378. doi: 10.1016/0019-1035(81)90041-5

Clow, G. D. (1987). Generation of liquid water on Mars through the melting of a dusty snowpack. *Icarus*, 72(1), 95–127. doi: 10.1016/0019-1035(87)90123-0

Clow, G. D., McKay, C. P., Simmons, G. M., & Wharton, R. A. (1988). Climatological Observations and Predicted Sublimation Rates at Lake Hoare, Antarctica. *Journal of Climate*, 1(7), 715–728. doi: 10.1175/1520-0442(1988)001<0715:coapsr>2.0.co;2

Colaïtis, A., Spiga, A., Hourdin, F., Rio, C., Forget, F., & Millour, E. (2013). A thermal plume model for the Martian convective boundary layer. *Journal of Geophysical Research: Planets*, 118(7), 1468–1487. doi: doi.org/10.1002/jgre.20104

Conway, S. J., & Stillman, D. E. (2021). The role of liquid water in recent surface processes on Mars. In *Mars geological enigmas* (p. 207–261). Elsevier. doi: 10.1016/b978-0-12-820245-6.00009-4

Costard, F., Forget, F., Mangold, N., & Peulvast, J. P. (2002). Formation of Recent Martian Debris Flows by Melting of Near-Surface Ground Ice at High Obliquity. *Science*, 295(5552), 110–113. doi: 10.1126/science.1066698

de Haas, T., Conway, S. J., Butcher, F. E. G., Levy, J., Grindrod, P. M., Goudge, T. A., & Balme, M. R. (2019, January). Time will tell: temporal evolution of Martian gullies and palaeoclimatic implications. *Geological Society of London Special Publications*, 467(1), 165–186. doi: 10.1144/SP467.1

Dickson, J. L., Palumbo, A. M., Head, J. W., Kerber, L., Fassett, C. I., & Kreslavsky, M. A. (2023). Gullies on Mars could have formed by melting of water ice during periods of high obliquity. *Science*, 380(6652), 1363–1367. doi: 10.1126/science.abk2464

Douglas, T. A., & Mellon, M. T. (2019). Sublimation of terrestrial permafrost and the implications for ice-loss processes on Mars. *Nature Communications*, 10(1). doi: 10.1038/s41467-019-09410-8

Dundas, C. M., Bramson, A. M., Ojha, L., Wray, J. J., Mellon, M. T., Byrne, S., ... Holt, J. W. (2018). Exposed subsurface ice sheets in the Martian mid-latitudes. *Science*, 359(6372), 199–201. doi: 10.1126/science.aoa1619

Dundas, C. M., Byrne, S., McEwen, A. S., Mellon, M. T., Kennedy, M. R., Daubar, I. J., & Saper, L. (2014). HiRISE observations of new impact craters exposing Martian ground ice. *Journal of Geophysical Research: Planets*, 119(1), 109–127. doi: 10.1002/2013je004482

Dundas, C. M., Conway, S. J., & Cushing, G. E. (2022). Martian gully activity and the gully sediment transport system. *Icarus*, 386, 115133. doi: 10.1016/j.icarus.2022.115133

Dundas, C. M., Diniega, S., Hansen, C. J., Byrne, S., & McEwen, A. S. (2012). Seasonal activity and morphological changes in martian gullies. *Icarus*, 220(1), 124–143. doi: 10.1016/j.icarus.2012.04.005

Dundas, C. M., McEwen, A. S., Diniega, S., Hansen, C. J., Byrne, S., & McElwaine, J. N. (2019). The formation of gullies on Mars today. *Geological Society of London Special Publications*, 467, 67–94. doi: 10.1144/SP467.5

Dundas, C. M., Mellon, M. T., Conway, S. J., Daubar, I. J., Williams, K. E., Ojha, L., ... Pathare, A. V. (2021). Widespread Exposures of Extensive Clean Shallow Ice in the Midlatitudes of Mars. *Journal of Geophysical Research: Planets*, 126(3). doi: 10.1029/2020je006617

England, D. E., & McNider, R. T. (1995). Stability functions based upon shear functions. *Boundary-Layer Meteorology*, 74(1–2), 113–130. doi: 10.1007/bf00715713

Fairall, C. W., Bradley, E. F., Hare, J. E., Grachev, A. A., & Edson, J. B. (2003). Bulk Parameterization of Air–Sea Fluxes: Updates and Verification for the COARE Algorithm. *Journal of Climate*, 16(4), 571–591. doi: 10.1175/1520-0442(2003)016<0571:bpoaf>2.0.co;2

Fairall, C. W., Bradley, E. F., Rogers, D. P., Edson, J. B., & Young, G. S. (1996).

Bulk parameterization of air-sea fluxes for Tropical Ocean-Global Atmosphere Coupled-Ocean Atmosphere Response Experiment. *Journal of Geophysical Research: Oceans*, 101(C2), 3747–3764. doi: 10.1029/95jc03205

Fassett, C. I., & Head, J. W. (2008). The timing of martian valley network activity: Constraints from buffered crater counting. *Icarus*, 195(1), 61–89. doi: 10.1016/j.icarus.2007.12.009

Fitzpatrick, N., Radić, V., & Menounos, B. (2017). Surface Energy Balance Closure and Turbulent Flux Parameterization on a Mid-Latitude Mountain Glacier, Purcell Mountains, Canada. *Frontiers in Earth Science*, 5. doi: 10.3389/feart.2017.00067

Forget, F., Hourdin, F., Fournier, R., Hourdin, C., Talagrand, O., Collins, M., ... Huot, J.-P. (1999). Improved general circulation models of the martian atmosphere from the surface to above 80 km. *Journal of Geophysical Research: Planets*, 104(E10), 24155–24175. doi: 10.1029/1999JE001025

Forget, F., Millour, E., & the Mars PCM Developpement team. (2025). *Mars Planetary Climate Model [Software]*.

Glavin, D. P., Freissinet, C., Miller, K. E., Eigenbrode, J. L., Brunner, A. E., Buch, A., ... Mahaffy, P. R. (2013). Evidence for perchlorates and the origin of chlorinated hydrocarbons detected by SAM at the Rocknest aeolian deposit in Gale Crater. *Journal of Geophysical Research: Planets*, 118(10), 1955–1973. doi: 10.1002/jgre.20144

Golombek, M., Warner, N. H., Grant, J. A., Hauber, E., Ansan, V., Weitz, C. M., ... Banerdt, W. B. (2020). Geology of the InSight landing site on Mars. *Nature Communications*, 11(1). doi: 10.1038/s41467-020-14679-1

Haberle, R. M., McKay, C. P., Schaeffer, J., Cabrol, N. A., Grin, E. A., Zent, A. P., & Quinn, R. (2001). On the possibility of liquid water on present-day Mars. *Journal of Geophysical Research: Planets*, 106(E10), 23317–23326. doi: 10.1029/2000je001360

Harrison, T. N., Osinski, G. R., Tornabene, L. L., & Jones, E. (2015). Global documentation of gullies with the Mars Reconnaissance Orbiter Context Camera and implications for their formation. *Icarus*, 252, 236–254. doi: 10.1016/j.icarus.2015.01.022

Hébrard, E., Listowski, C., Coll, P., Marticorena, B., Bergametti, G., Määttänen, A., ... Forget, F. (2012). An aerodynamic roughness length map derived from extended Martian rock abundance data. *Journal of Geophysical Research (Planets)*, 117(E4), E04008. doi: 10.1029/2011JE003942

Hecht, M. H. (2002). Metastability of Liquid Water on Mars. *Icarus*, 156(2), 373–386. doi: 10.1006/icar.2001.6794

Hecht, M. H., Kounaves, S. P., Quinn, R. C., West, S. J., Young, S. M. M., Ming, D. W., ... Smith, P. H. (2009). Detection of Perchlorate and the Soluble Chemistry of Martian Soil at the Phoenix Lander Site. *Science*, 325(5936), 64–67. doi: 10.1126/science.1172466

Hobbs, P. V. (1974). *Ice physics*. New York: Oxford Univ. Press.

Hudson, T. L., & Aharonson, O. (2008). Diffusion barriers at Mars surface conditions: Salt crusts, particle size mixtures, and dust. *Journal of Geophysical Research: Planets*, 113(E9). doi: 10.1029/2007je003026

Hudson, T. L., Aharonson, O., Schorghofer, N., Farmer, C. B., Hecht, M. H., & Bridges, N. T. (2007). Water vapor diffusion in Mars subsurface environments. *Journal of Geophysical Research (Planets)*, 112(E5), E05016. doi: 10.1029/2006JE002815

Ingersoll, A. P. (1970). Mars: Occurrence of Liquid Water. *Science*, 168(3934), 972–973. doi: 10.1126/science.168.3934.972

Kahre, M. A., Murphy, J. R., Newman, C. E., Wilson, R. J., Cantor, B. A., Lemmon, M. T., & Wolff, M. J. (2017). The Mars dust cycle. In R. M. Haberle, R. T. Clancy, F. Forget, M. D. Smith, & R. W. Zurek (Eds.), *The atmo-*

sphere and climate of Mars (p. 295–337). Cambridge University Press. doi: 10.1017/9781139060172.010

Khuller, A. R., & Christensen, P. R. (2021). Evidence of Exposed Dusty Water Ice within Martian Gullies. *Journal of Geophysical Research: Planets*, 126(2). doi: 10.1029/2020je006539

Khuller, A. R., Christensen, P. R., & Warren, S. G. (2021). Spectral albedo of dusty martian h₂o snow and ice. *Journal of Geophysical Research: Planets*, 126(9). doi: 10.1029/2021je006910

Khuller, A. R., & Clow, G. D. (2024). Turbulent Fluxes and Evaporation/Sublimation Rates on Earth, Mars, Titan, and Exoplanets. *Journal of Geophysical Research: Planets*, 129(4). doi: 10.1029/2023je008114

Khuller, A. R., Warren, S. G., Christensen, P. R., & Clow, G. D. (2024). Potential for photosynthesis on Mars within snow and ice. *Communications Earth & Environment*, 5(1). doi: 10.1038/s43247-024-01730-y

Kossacki, K. J., & Markiewicz, W. J. (2004). Seasonal melting of surface water ice condensing in martian gullies. *Icarus*, 171(2), 272–283. doi: 10.1016/j.icarus.2004.05.018

Kreslavsky, M. A., & Head, J. W. (2003). North–south topographic slope asymmetry on mars: Evidence for insolation-related erosion at high obliquity. *Geophysical Research Letters*, 30(15). doi: 10.1029/2003gl017795

Lalich, D. E., Holt, J. W., & Smith, I. B. (2019). Radar Reflectivity as a Proxy for the Dust Content of Individual Layers in the Martian North Polar Layered Deposits. *Journal of Geophysical Research: Planets*, 124(7), 1690–1703. doi: 10.1029/2018je005787

Lange, L., & Forget, F. (2025). *Replication Data for: On the Possibility of Melting Water Ice during the Recent Past of Mars. Application to the Formation of Gullies. [Dataset]*. Harvard Dataverse. doi: <https://doi.org/10.7910/DVN/SMJDHJ>

Lange, L., Forget, F., Dupont, E., Vandemeulebrouck, R., Spiga, A., Millour, E., ... Bierjon, A. (2023). Modeling slope microclimates in the mars planetary climate model. *Journal of Geophysical Research: Planets*, 128(10). doi: 10.1029/2023je007915

Lange, L., Forget, F., Vincendon, M., Spiga, A., Vos, E., Aharonson, O., ... Vandemeulebrouck, R. (2023). A Reappraisal of Subtropical Subsurface Water Ice Stability on Mars. *Geophysical Research Letters*, 50(21), e2023GL105177. doi: 10.1029/2023GL105177

Lange, L., Piqueux, S., Edwards, C. S., Forget, F., Naar, J., Vos, E., & Szantai, A. (2024). Observations of Water Frost on Mars With THEMIS: Application to the Presence of Brines and the Stability of (Sub)Surface Water Ice. *Journal of Geophysical Research: Planets*, 129(10). doi: 10.1029/2024je008489

Langevin, Y., Bibring, J., Montmessin, F., Forget, F., Vincendon, M., Douté, S., ... Gondet, B. (2007). Observations of the south seasonal cap of Mars during recession in 2004–2006 by the OMEGA visible/near-infrared imaging spectrometer on board Mars Express. *Journal of Geophysical Research: Planets*, 112(E8). doi: 10.1029/2006je002841

Langevin, Y., Poulet, F., Bibring, J. P., Schmitt, B., Douté, S., & Gondet, B. (2005). Summer Evolution of the North Polar Cap of Mars as Observed by OMEGA/Mars Express. *Science*, 307(5715), 1581–1584. doi: 10.1126/science.1109438

Laskar, J., Correia, A., Gastineau, M., Joutel, F., Levrard, B., & Robutel, P. (2004). Long term evolution and chaotic diffusion of the insolation quantities of Mars. *Icarus*, 170(2), 343–364. doi: 10.1016/j.icarus.2004.04.005

Madeleine, J. B., Head, J. W., Forget, F., Navarro, T., Millour, E., A., ... Dickson, J. L. (2014). Recent Ice Ages on Mars: The role of radiatively active clouds and cloud microphysics. *Geophysical Research Letters*, 41(14), 4873–4879. doi:

10.1002/2014GL059861

Malin, M. C., & Edgett, K. S. (2000). Evidence for Recent Groundwater Seepage and Surface Runoff on Mars. *Science*, 288(5475), 2330–2335. doi: 10.1126/science.288.5475.2330

Malin, M. C., & Edgett, K. S. (2003). Evidence for Persistent Flow and Aqueous Sedimentation on Early Mars. *Science*, 302(5652), 1931–1934. doi: 10.1126/science.1090544

Malin, M. C., Edgett, K. S., Posiolova, L. V., McColley, S. M., & Dobrea, E. Z. N. (2006). Present-Day Impact Cratering Rate and Contemporary Gully Activity on Mars. *Science*, 314(5805), 1573–1577. doi: 10.1126/science.1135156

Mangold, N., Gupta, S., Gasnault, O., Dromart, G., Tarnas, J. D., Sholes, S. F., ... Williford, K. H. (2021). Perseverance rover reveals an ancient delta-lake system and flood deposits at Jezero crater, Mars. *Science*, 374(6568), 711–717. doi: 10.1126/science.abl4051

McKay, C. P., Mellon, M. T., & Friedmann, E. I. (1998). Soil temperatures and stability of ice-cemented ground in the McMurdo Dry Valleys, Antarctica. *Antarctic Science*, 10(1), 31–38. doi: 10.1017/s0954102098000054

Mellon, M. T., Feldman, W. C., & Prettyman, T. H. (2004). The presence and stability of ground ice in the southern hemisphere of Mars. *Icarus*, 169(2), 324–340. doi: 10.1016/j.icarus.2003.10.022

Mellon, M. T., & Phillips, R. J. (2001). Recent gullies on Mars and the source of liquid water. *Journal of Geophysical Research: Planets*, 106(E10), 23165–23179. doi: 10.1029/2000je001424

Möhlmann, D. T. (2008). The influence of van der Waals forces on the state of water in the shallow subsurface of Mars. *Icarus*, 195(1), 131–139. doi: 10.1016/j.icarus.2007.11.026

Montmessin, F., Smith, M. D., Langevin, Y., Mellon, M. T., & Fedorova, A. (2017). The Water Cycle. In R. M. Haberle, R. T. Clancy, F. Forget, M. D. Smith, & R. W. Zurek (Eds.), *Asteroids, comets, meteors - acm2017* (p. 295–337). doi: 10.1017/978139060172.011

Morgan, G. A., Head, J. W., Forget, F., Madeleine, J.-B., & Spiga, A. (2010). Gully formation on Mars: Two recent phases of formation suggested by links between morphology, slope orientation and insolation history. *Icarus*, 208(2), 658–666. doi: 10.1016/j.icarus.2010.02.019

Murphy, D. M., & Koop, T. (2005). Review of the vapour pressures of ice and super-cooled water for atmospheric applications. *Quarterly Journal of the Royal Meteorological Society*, 131(608), 1539–1565. doi: 10.1256/qj.04.94

Navarro, T., Madeleine, J.-B., Forget, F., Spiga, A., Millour, E., Montmessin, F., & Määttänen, A. (2014). Global climate modeling of the martian water cycle with improved microphysics and radiatively active water ice clouds. *Journal of Geophysical Research: Planets*, 119(7), 1479–1495. doi: 10.1002/2013je004550

Noblet, A., Conway, S., & Osinski, G. (2024). A global map of gullied hillslopes on Mars. *Icarus*, 418, 116147. doi: 10.1016/j.icarus.2024.116147

Phillips, R. J., Davis, B. J., Tanaka, K. L., Byrne, S., Mellon, M. T., Putzig, N. E., ... Seu, R. (2011). Massive co2 ice deposits sequestered in the south polar layered deposits of mars. *Science*, 332(6031), 838–841. doi: 10.1126/science.1203091

Pilotget, C., & Forget, F. (2016). Formation of gullies on Mars by debris flows triggered by CO₂ sublimation. *Nature Geoscience*, 9, 65–69. doi: 10.1038/ngeo2619

Pilotget, C., Forget, F., Millour, E., Vincendon, M., & Madeleine, J. (2011). Dark spots and cold jets in the polar regions of Mars: New clues from a thermal model of surface CO₂ ice. *Icarus*, 213(1), 131–149. doi: 10.1016/j.icarus.2011.01.031

Piqueux, S., & Christensen, P. R. (2009a). A model of thermal conductivity for planetary soils: 1. theory for unconsolidated soils. *Journal of Geophysical Research (Planets)*, 114(E9). doi: 10.1029/2008je003308

Piqueux, S., & Christensen, P. R. (2009b). A model of thermal conductivity for planetary soils: 2. theory for cemented soils. *Journal of Geophysical Research (Planets)*, 114(E9). doi: 10.1029/2008je003309

Plaut, J. J., Picardi, G., Safaeinili, A., Ivanov, A. B., Milkovich, S. M., Cicchetti, A., ... Edenhofer, P. (2007). Subsurface Radar Sounding of the South Polar Layered Deposits of Mars. *Science*, 316(5821), 92–95. doi: 10.1126/science.1139672

Poulet, F., Bibring, J.-P., Mustard, J. F., Gendrin, A., Mangold, N., Langevin, Y., ... Gomez, C. (2005). Phyllosilicates on Mars and implications for early martian climate. *Nature*, 438(7068), 623–627. doi: 10.1038/nature04274

Putzig, N. E., & Mellon, M. T. (2007). Apparent thermal inertia and the surface heterogeneity of Mars. *Icarus*, 191(1), 68–94. doi: 10.1016/j.icarus.2007.05.013

Rangarajan, V., Tornabene, L., Osinski, G., Dundas, C., Beyer, R., Herkenhoff, K., ... Dapremont, A. (2024). Novel quantitative methods to enable multispectral identification of high-purity water ice exposures on mars using high resolution imaging science experiment (hirise) images. *Icarus*, 419, 115849. doi: 10.1016/j.icarus.2023.115849

Reufer, A., Thomas, N., Benz, W., Byrne, S., Bray, V., Dundas, C., & Searls, M. (2010). Models of high velocity impacts into dust-covered ice: Application to Martian northern lowlands. *Planetary and Space Science*, 58(10), 1160–1168. doi: 10.1016/j.pss.2010.04.008

Rivera-Valentín, E. G., Chevrier, V. F., Soto, A., & Martínez, G. (2020). Distribution and habitability of (meta)stable brines on present-day Mars. *Nature Astronomy*, 4(8), 756–761. doi: 10.1038/s41550-020-1080-9

Rothschild, L. J., & Mancinelli, R. L. (2001). Life in extreme environments. *Nature*, 409(6823), 1092–1101. doi: 10.1038/35059215

Savijärvi, H., Polkko, J., Hieto, M., Martinez, G., Zorzano, M.-P., Tamppari, L., ... Harri, A.-M. (2024). Wintertime column modeling in Jezero crater, Mars: Period of near-fog and a dust event. *Icarus*, 421, 116242. doi: 10.1016/j.icarus.2024.116242

Schorghofer, N. (2020). Mars: Quantitative Evaluation of Crocus Melting behind Boulders. *The Astrophysical Journal*, 890(1), 49. doi: 10.3847/1538-4357/ab612f

Schorghofer, N., & Aharonson, O. (2005). Stability and exchange of subsurface ice on Mars. *Journal of Geophysical Research: Planets*, 110(E5). doi: 10.1029/2004JE002350

Schorghofer, N., Levy, J., & Goudge, T. (2019). High-Resolution Thermal Environment of Recurring Slope Lineae in Palikir Crater, Mars, and Its Implications for Volatiles. *Journal of Geophysical Research: Planets*, 124(11), 2852–2862. doi: 10.1029/2019je006083

Siegler, M., Aharonson, O., Carey, E., Choukroun, M., Hudson, T., Schorghofer, N., & Xu, S. (2012). Measurements of thermal properties of icy Mars regolith analogs. *Journal of Geophysical Research: Planets*, 117(E3). doi: 10.1029/2011JE003938

Singh, D., & Flanner, M. G. (2016). An improved carbon dioxide snow spectral albedo model: Application to martian conditions. *Journal of Geophysical Research: Planets*, 121(10), 2037–2054. doi: 10.1002/2016je005040

Smith, I. B., & Spiga, A. (2018). Seasonal variability in winds in the north polar region of mars. *Icarus*, 308, 188–196. doi: 10.1016/j.icarus.2017.10.005

Smith, M. D. (2002). The annual cycle of water vapor on Mars as observed by the Thermal Emission Spectrometer. *Journal of Geophysical Research: Planets*,

ets, 107(E11), 25-1-25-19. doi: 10.1029/2001JE001522

Spiga, A., & Smith, I. (2018). Katabatic jumps in the martian northern polar regions. *Icarus*, 308, 197–208. doi: 10.1016/j.icarus.2017.10.021

Toner, J., Catling, D., & Light, B. (2015). A revised Pitzer model for low-temperature soluble salt assemblages at the Phoenix site, Mars. *Geochimica et Cosmochimica Acta*, 166, 327–343. doi: 10.1016/j.gca.2015.06.011

Vincendon, M., Forget, F., & Mustard, J. (2010b). Water ice at low to midlatitudes on Mars. *Journal of Geophysical Research (Planets)*, 115(E10), E10001. doi: 10.1029/2010JE003584

Williams, K., Toon, O., Heldmann, J., & Mellon, M. (2009). Ancient melting of mid-latitude snowpacks on Mars as a water source for gullies. *Icarus*, 200(2), 418–425. doi: 10.1016/j.icarus.2008.12.013

Williams, K. E., Toon, O. B., Heldmann, J. L., McKay, C., & Mellon, M. T. (2008). Stability of mid-latitude snowpacks on Mars. *Icarus*, 196(2), 565–577. doi: 10.1016/j.icarus.2008.03.017

Williams, R. M. E., Grotzinger, J. P., Dietrich, W. E., Gupta, S., Sumner, D. Y., Wiens, R. C., ... Moores, J. E. (2013). Martian Fluvial Conglomerates at Gale Crater. *Science*, 340(6136), 1068–1072. doi: 10.1126/science.1237317

Wood, S. E., & Griffiths, S. D. (2007). Mars Subsurface Warming at Low Obliquity. In LPI Editorial Board (Ed.), *Seventh international conference on mars* (Vol. 1353, p. 3387). Retrieved from <https://www.hou.usra.edu/meetings/8thmars2014/pdf/1495.pdf>

Zuber, M. T., Phillips, R. J., Andrews-Hanna, J. C., Asmar, S. W., Konopliv, A. S., Lemoine, F. G., ... Smrekar, S. E. (2007). Density of Mars' South Polar Layered Deposits. *Science*, 317(5845), 1718–1719. doi: 10.1126/science.1146995